Dynamic Interplay Between Kerr Combs and Brillouin Lasing in Fiber Cavities

Erwan Lucas, Moise Deroh, Bertrand Kibler

Dynamic Interplay Between Kerr Combs and Brillouin Lasing in Fiber Cavities

Erwan Lucas,[1,*] Moise Deroh,[1] and Bertrand Kibler[1]

[1] *Laboratoire Interdisciplinaire Carnot de Bourgogne (ICB), UMR6303 CNRS-UB, 21078 Dijon, France*

Highly coherent frequency comb are of crucial importance for optical synthesis and metrology, spectroscopy, laser ranging and optical communications. Kerr combs, generated via cascaded nonlinear frequency conversion in a passive optical cavity, typically offer high repetition rates, which is essential for some of these applications. Recently, new ways of generating Kerr combs combining Kerr and Brillouin effects have emerged with the aim of improving some performances, especially in the fiber cavity platform. Direct coherent pumping is replaced by lasing on specific cavity modes, offering easily adjustable repetition rates and enhanced coherence by Brillouin purification. Here, we investigate such a system, implemented in a nonreciprocal cavity. Highly coherent combs are demonstrated by finely controlling the bichromatic Brillouin lasing and the Kerr comb parameters. We provide a suitable numerical model that accounts for the interplay between Brillouin scattering, Kerr effect, and cavity resonant feedback. Quantitative agreements with experiments reveal the importance of the pump lasers detuning in setting the comb's properties, through the mode pulling effect. This phenomenon, along with multimode lasing that impedes the coherence, was not studied in previous fiber-based demonstrations. We discuss these limitations and devise several scaling laws.

Optical frequency combs, whose broadband spectrum is composed of equi-spaced coherent frequency tones, are very powerful tools in a wide range of fields including frequency metrology, microwaves generation and spectroscopy [1, 2]. Various technologies can be used to generate such OFCs, such as nonlinear frequency conversion in passive optical resonators, known as Kerr combs [3]. These combs are traditionally generated by coherently driving an optical cavity with a continuous-wave (CW) laser coupled into one of its resonances. The intricate balance between dispersion, losses, and non-linearities leads to the formation of optical patterns in the cavity field, such as the dissipative Kerr soliton in anomalous group-velocity dispersion (GVD) [3]. When the pattern circulates stably in the resonator, the output pulse train constitutes an OFC.

In this contribution, we study a hybrid system based on a bichromatic Brillouin fiber laser to generate a Kerr comb. Similar schemes have recently been experimentally demonstrated in fiber cavities [4, 5] and microresonators [6, 7]. However, a detailed description of the dynamical interplay between Brillouin lasing and Kerr comb generation remains elusive, especially in nonreciprocal fiber cavities. Here, we investigate these systems in depth, accounting for the Brillouin gain's complex nature, and highlight the pump detuning as a key parameter. Most importantly, we distinguish between stable single-frequency Brillouin lasing regimes, producing low-noise Kerr combs, and noisy regimes, where lasing occurs in multiple cavity modes.

Figure 1a presents the experimental setup and its operating principle. The fiber cavity is closed by an optical circulator, a typical configuration for Brillouin lasers [8, 9]. Thus, the pump lasers propagate on a

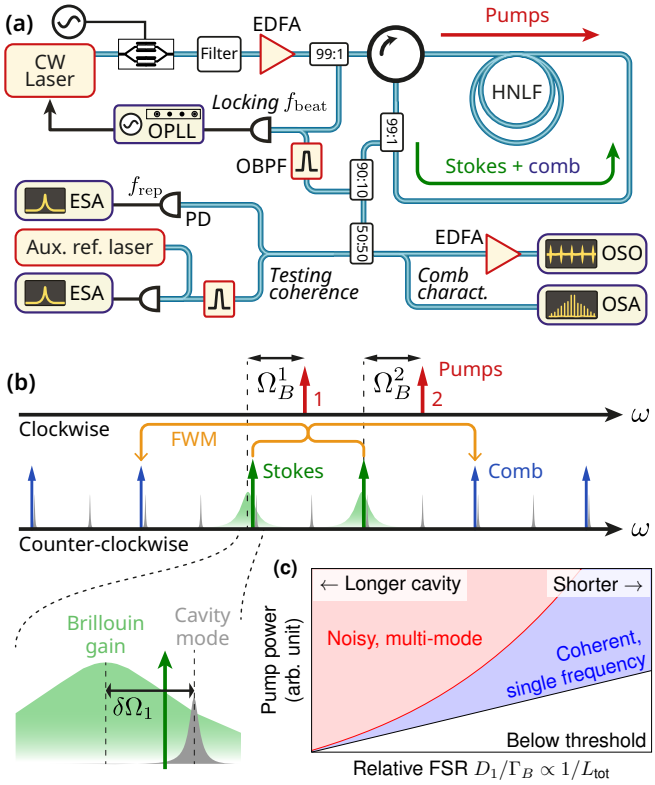

Figure 1: **Kerr comb in fiber cavity Brillouin laser**. **(a)** Experimental setup. EDFA: Erbium-doped fiber amplifier, HNLF: Highly nonlinear fiber, PD: Photodiode, OPLL: Optical phase lock loop, OBPF: Optical bandpass filter, ESA: Electronic spectrum analyzer, OSA: Optical spectrum analyzer, OSO: Optical sampling oscilloscope **(b)** Principle of Brillouin-Kerr comb generation. **(c)** Simplified stability chart of the lasing states, as a function of the cavity FSR relative to the Brillouin gain bandwidth, and of the pump power.

* erwan.lucas@u-bourgogne.fr

single pass and are not subject to any clockwise resonance conditions. This allows for efficient pumps injection, while relaxing the requirements on their linewidth, which can exceed the very high-quality factor resonances of the fiber cavity. These pumps induce counterclockwise Brillouin Stokes gains, which are down-shifted by the phonon frequency $\Omega_B/2\pi$. When the gain overcomes losses, Stokes waves can resonate and build up to form laser lines, which in turn produce a comb via cascaded four-wave mixing. A highly nonlinear fiber (HNLF) is used to enhance Brillouin and Kerr nonlinearities. Moreover, Brillouin-Stokes lasers feature a linewidth narrowing relative to their pump [10, 11], potentially enhancing the comb coherence.

We only consider the case of net normal cavity GVD, where comb formation via dual pumping is possible [12], to avoid modulation instability occurring in the anomalous dispersion regime, whose random nature could interfere with our discussion on the laser dynamics.

MODEL

We developed a specific model to describe our system, based on a set of coupled equations derived from the Ikeda map [13], under the slow varying envelope approximation, and in the retarded frame [14]. At each roundtrip, two successive steps are performed. First, the Brillouin scattering *steady state* is computed by solving the equations

$$\frac{d\left|A^j\right|^2}{dz} = \left(-\frac{\mathrm{Re}\left[g_B(\delta\Omega_j)\right]}{A_{\mathrm{eff}}}\left|\tilde{A}_{\mu_j}\right|^2 - \alpha\right)\left|\mathrm{A}^j\right|^2 \quad (1)$$

$$-\frac{d\left|\tilde{A}_{\mu_j}\right|^2}{dz} = \left(\frac{\mathrm{Re}\left[g_B(\delta\Omega_j)\right]}{A_{\mathrm{eff}}}\left|A^j\right|^2 - \alpha\right)\left|\tilde{A}_{\mu_j}\right|^2 \quad (2)$$

$$\left|A^j(L)\right|^2 = P^p_{\mathrm{in}} \qquad \text{and} \qquad \tilde{A}^{(n)}_{\mu_j}(0) = \tilde{A}^{(n-1)}_{\mu_j}(L) \quad (3)$$

$$g_B(\delta\Omega) = \frac{g_B^0}{1 + 2i\,\delta\Omega/\Gamma_B} \quad (4)$$

where $\left|A^j\right|^2$ and $\left|\tilde{A}_{\mu_j}\right|^2$ are the pump and corresponding Stokes powers.

$$\mu_j = \frac{(-1)^j \Delta\omega_p/2 - \Omega_B}{D_1} \quad (5)$$

is the relative mode number of the cavity modes experiencing Stokes lasing. The index $j = 1, 2$ accounts for each pump, $\Delta\omega_p$ is the pumps frequency spacing and $D_1/2\pi$ is the cavity's free spectral range (FSR). α is the attenuation coefficient and is neglected compared to the discrete cavity losses η (circulator, coupler, splices). Γ_B is the Brillouin gain bandwidth, while $\delta\Omega$ is the mismatch between the Brillouin gain peak and the nearest lasing mode, which can be controlled by tuning the pump laser frequency. We solve this step numerically using a boundary value problem solver [15] initialized with an analytical expression that assumes pump non-depletion [16]. This provides the spatial distribution of the pump power $A^j(z)$ for the next step. Note that other simulation techniques are available to compute the dynamical response of the Brillouin laser [17, 18]. While these methods may be useful for modeling Brillouin gain competition and multimode Brillouin operation, they may not be suitable for incorporating dispersive effects and are more computationally intensive.

Second, the following modified Nonlinear Schrödinger Equation (NLSE) is integrated using the split-step Fourier method:

$$\begin{aligned}\frac{\partial\tilde{A}_\mu}{\partial z} = &\left[-\frac{\alpha}{2} - i\frac{\beta_2}{2}\omega_\mu^2\right]\tilde{A}_\mu + i\gamma_0\ \mathcal{F}\left[\left|A\right|^2 A\right]_\mu \\ &+ \sum_{j=1,2}\frac{g_B(\delta\Omega_j)}{2\,A_{\mathrm{eff}}}\left|A^j(z)\right|^2\tilde{A}_\mu\,\delta_{\mu\mu_j}\end{aligned} \quad (6)$$

The equation is written in the frequency domain, μ represents the longitudinal mode number in the cavity. The Brillouin gain term is applied to the pumped Stokes modes $\mu_j,\ j \in 1, 2$ ($\delta_{\mu\mu_j}$ represents the Kronecker symbol). The operator $\mathcal{F}\left[\cdot\right]_\mu$ represents the μ^{th} component of the Fourier series.

Finally, after propagation, the out-coupling (ratio $\theta = 1\,\%$ in both cavities) and losses η are applied to iterate from roundtrip $n \to n+1$:

$$\tilde{A}^{(n+1)}_\mu(0) = \sqrt{\eta\ (1-\theta)}\,\tilde{A}^{(n)}_\mu(L) \quad (7)$$

EXPERIMENTAL VALIDATION

We studied two cavities (A,B) having different length, whose attributes are summarized in table I. To maintain normal net dispersion, we minimized the single-mode fiber (SMF) introduced by the coupling components.

Cavity	A	B	Unit
HNLF			
HNLF length L	10	60	m
Brillouin gain g_B^0/A_{eff}	3	3	$\mathrm{dB\,m^{-1}\,W^{-1}}$
Gain bandwidth $\Gamma_B/2\pi$	52	47	MHz
Nonlinearity γ	12.5	9	$\mathrm{W^{-1}\,km^{-1}}$
GVD D	−2.9	−0.55	$\mathrm{ps\,nm^{-1}\,km^{-1}}$
Global cavity parameters			
Residual SMF	1.2	5	m
Total cavity length L_{tot}	11.2	65	m
Total roundtrip loss η	−1.17	−1.22	dB
Loaded linewidth $\kappa/2\pi$	695	128	kHz
Free spectral range $D_1/2\pi$	18.39	3.15	MHz

Table I: Physical parameters of the cavities studied in this work. GVD: Group-velocity dispersion.

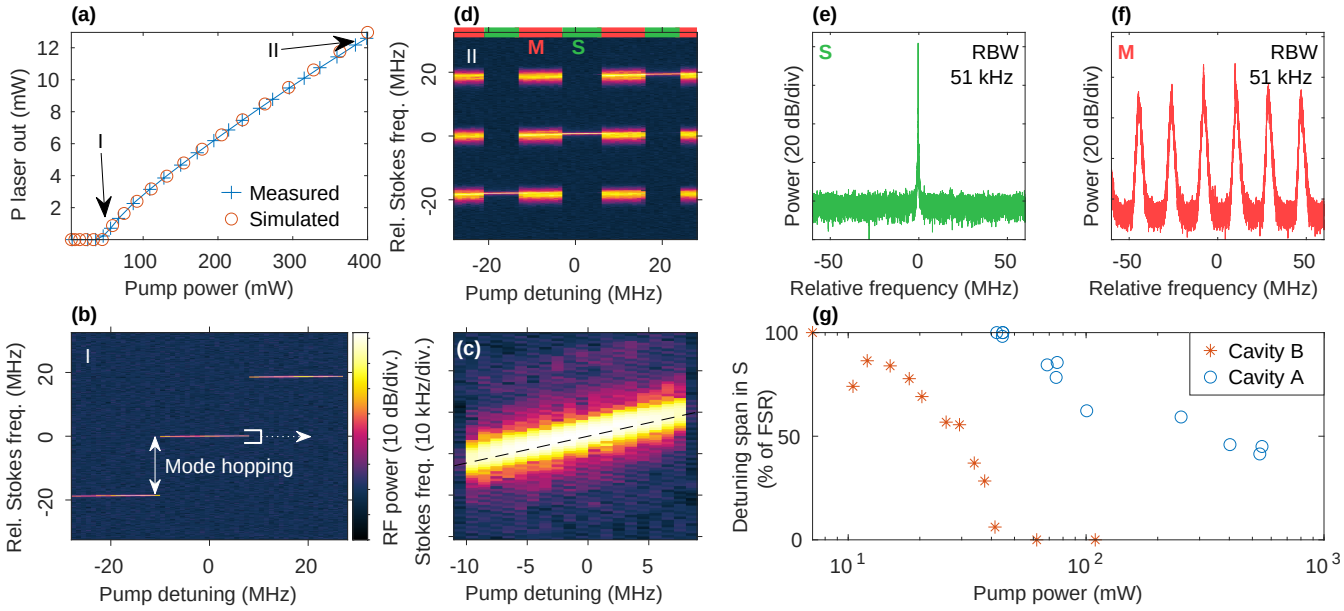

Figure 2: **Brillouin laser mode pulling and emission regimes characterization**. **(a)** Lasing threshold measurement in cavity A and simulation. **(b)** Stokes laser spectrum evolution with the pump detuning, near threshold (I). **(c)** Zoom-in on the step in (b), showing the mode pulling effect. **(d)** Stokes laser spectrum evolution with pump detuning at higher power (II). The laser is multimode around mode-hopping regions (red, M), while the detuning range with single-mode emission (green, S) shrinks with increased power. **(e)** Stokes laser – pump laser beatnote in the single-mode lasing regime. **(f)** Same beatnote in the multimode lasing regime. **(g)** Evolution of the pump detuning range for single frequency emission (S) with the pump power for the two different cavity lengths.

Brillouin laser characterization

First, we characterize the Brillouin laser with a single pump, thus disabling Kerr comb generation. The measured threshold of 42 mW in cavity A (see fig. 2a), is notably larger that that of the longer cavity B (7.5 mW).

The values obtained $g_B/A_{\text{eff}} \sim 3\,\text{dB}\,\text{W}^{-1}\,\text{m}^{-1}$ and $\Omega_B/2\pi \sim 9.1\,\text{GHz}$ are in agreement with typical characteristics of HNLF [19].

We then characterize the Stokes lasing frequency as a function of the Brillouin gain detuning. To accurately control $\delta\Omega$, we implement an offset sideband-locking [20] scheme, illustrated on fig. 3. Pound-Drever-Hall locking is employed to stabilize the seed laser to the cavity in the counterclockwise direction, while maintaining low injected power in the cavity coupler to prevent crosstalk. The Brillouin pump is generated by electro-optic modulation of the seed laser, followed by bandpass filtering to create a single sideband, which is amplified and then injected in the clockwise direction through the circulator. Thus, the frequency of the Brillouin pump relative to the cavity, and consequently $\delta\Omega$, is controlled using the synthesizer used for sideband generation (ω_{synth}). Monitoring the beatnote ω_{beat} between the Stokes laser and pump sideband then allows us to precisely track the emission frequency of the Brillouin laser, while scanning $\delta\Omega$. The variation of the Stokes emission frequency can then

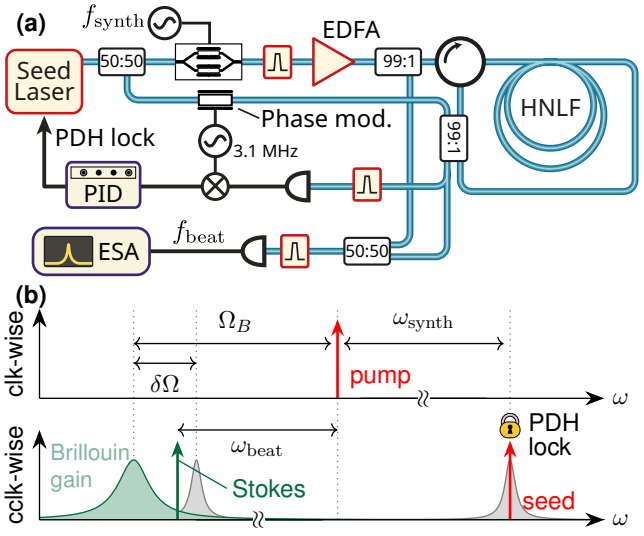

Figure 3: **Detuning scan in a Brillouin laser**. **(a)** Experimental setup for offset sideband-locking and emission frequency monitoring. **(b)** Principle of the offset sideband-locking for the Brillouin gain detuning scan.

be expressed as $\Delta\omega_{\text{Stokes}} = \xi\Delta\omega_{\text{synth}} - \Delta\omega_{\text{beat}}$, where $\xi = -1$ since we selected the lower frequency sideband.

Figure 2b shows the tuning of the laser frequency in

cavity A near the lasing threshold. Mode hopping is visible when the emission frequency switches from one longitudinal mode to another, stepping by one cavity FSR. Focusing on a range sustained by a single longitudinal mode reveals that the emission frequency shifts linearly as a function of $\delta\Omega$ (fig. 2c). This phenomenon is known as mode pulling and stems from the imaginary part of the Brillouin gain, in agreement with the Kramers-Kronig relations [7, 21, 22]. Consequently, the laser emission is steered toward the peak of the gain lobe. The mode pulling slope is fitted and follows the expression [23]

$$\frac{\partial\omega_{\text{Stokes}}}{\partial\delta\Omega} = \frac{1}{1+\Gamma_B/\kappa} = 1.33\times10^{-2}, \tag{8}$$

yielding the ratio of the Brillouin gain bandwidth to the cavity linewidth $\Gamma_B/\kappa = 74$. As κ was measured, we obtain $\Gamma_B/2\pi = 52\,\text{MHz}$ and a similar value for cavity B, which is typical for HNLF [19].

At higher power (fig. 2d), the laser dynamics changes significantly around the mode-hopping transitions. The emission goes from single mode at small detuning (S-regime, shown in fig. 2e), to multimode at higher detuning (M-regime in fig. 2f). The energy is distributed across several cavity modes, and the laser coherence is strongly degraded. Note that multimode instabilities in Brillouin lasers have been extensively investigated, depending on the cavity parameters. They can lead to random fluctuations of the laser output [24–26], or even a form of mode-locking [27–31] in low-finesse cavities (weak feedback coupling), which was not observed here.

Importantly, the detuning range where the S-mode is maintained, gradually shrinks with increasing pump power, as shown in fig. 2g. Beyond a critical power, the laser operates purely in the M regime. Moreover, the longer the cavity, the lower the power at which the loss of stability occurs, since the number of modes under the gain curve becomes larger and their respective gains become similar, leading to simultaneous oscillations.

Comb generation

bichromatic pumping can be achieved by combining two continuous-wave lasers or, as shown in fig. 1a, by means of electro-optical modulation. We use a Mach-Zehnder intensity modulator in carrier-suppressed mode driven by a tunable signal from a synthesizer (at 20 GHz) to create two pumps with a tunable spacing $\Delta\omega_p/2\pi \approx 40\,\text{GHz}$ (much higher than the cavity's FSR). We use a programmable filter to select the first-order sidebands and further reject the carrier. To cancel the thermal drift of our cavity relative to the pump laser, we implement a phase-lock loop that frequency-locks f_{beat} of one pump with its Stokes laser [9].

Bichromatic pumping has the interesting feature of being thresholdless [32]. Initial parametric sidebands are observed when the Stokes lasing threshold is reached for both Stokes waves. The number of generated lines then increases with the injected power, as shown in fig. 4 and fig. 5e.

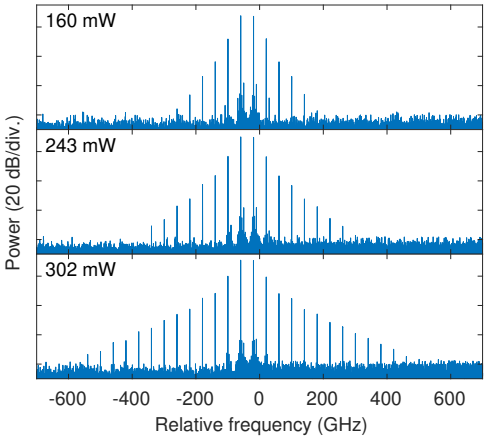

Figure 4: **Comb evolution with pump power**. Measured comb spectra obtained in cavity A, for increasing total pump power (indicated in the insets).

Figure 5a shows a comb generated in cavity A, for a total pump power of 421 mW. The pump spacing and lockpoint were chosen to preserve coherent single-mode emission and maximize comb bandwidth. The coherence of the comb is assessed by measuring a narrow beatnote at its repetition rate, and by beating the comb line -10 with an auxiliary low-noise laser. (fig. 5b). Interestingly, the repetition rate of the comb differs from the pump spacing. Since the phonon frequency is wavelength-dependent, Stokes 1 and 2 experience a different shift from their respective pump: $\Omega_B^j = \dfrac{n_j v_A}{\lambda_j}$, where n_j is the effective refractive index at the pump wavelength λ_j and v_A is the acoustic velocity. This effect amounts to $\Omega_B^2 - \Omega_B^1 \sim 2\,\text{MHz}$ in the present configuration.

Using the experimental parameters in our model, with small pump detunings ($\delta\Omega_1 = \delta\Omega_2 = -2\,\text{MHz}$), the simulated comb agrees remarkably well with the measured spectrum. Under normal net cavity dispersion, the temporal pattern in the cavity consists of a 'dark pulse' consisting of two switching waves [33] formed on the sinusoidal modulation pattern resulting from the two Stokes fields interference, as shown in fig. 5c. The temporal waveform measured on an optical sampling oscilloscope (OSO) (fig. 5d) agrees well with this prediction. Note that this latter technique can only be applied to the measurement of coherent temporal periodic signals, which further validates the comb coherence. The slight shape mismatch is likely caused by the optical amplifier before the OSO. Combs operating under normal dispersion are well-known for their high conversion efficiency. In our experiment, we measured a conversion efficiency of 22 %

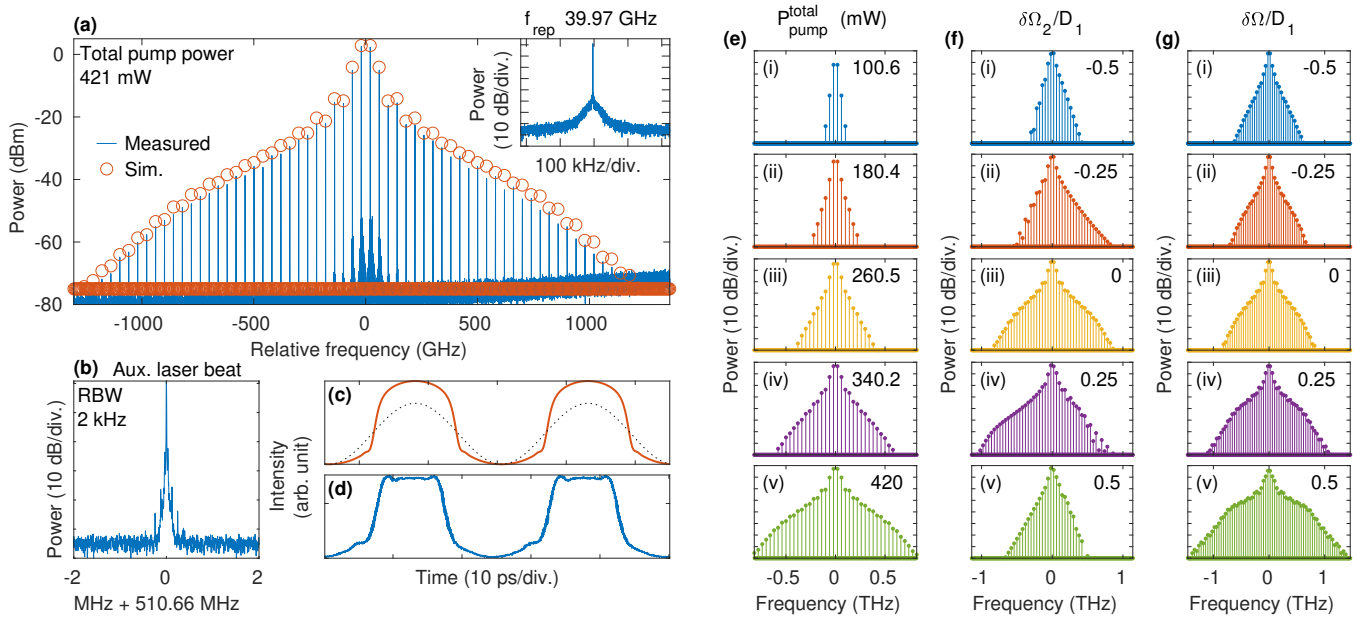

Figure 5: **Comb generation in single-mode regime and comb evolution**. **(a)** Optical spectrum of a comb obtained in cavity A, with 40 GHz pumps separation. The simulation result is overlaid (circles). The pump power is 421 mW. The noise 'pedestal' around the center comb lines is an artifact of the OSA (Apex AP2443B). The inset shows the repetition rate beatnote, with 100 Hz resolution bandwidth (RBW). **(b)** RF beatnote of comb line −10 with a reference auxiliary laser. **(c)** Simulated intra-cavity temporal intensity profile (solid), and pump interference pattern (dotted). **(d)** Temporal intensity profile corresponding to the comb in (a), measured on the OSO. **(e)** Simulated pump power sweep from 100 mW to 420 mW for $\delta\Omega_1 = \delta\Omega_2 = 0$. **(f)** Simulated scan of $\delta\Omega_2$ in $[-D_1/2, D_1/2]$, while $\delta\Omega_1 = 0$ is kept constant. The pump power is 420 mW. **(g)** Simulated detuning scan of $\delta\Omega = \delta\Omega_1 = \delta\Omega_2$ in $[-D_1/2, D_1/2]$ for a pump power of 420 mW.

from the Stokes lines to the rest of the comb, which exceeds that of bright solitons. However, the global conversion efficiency of our system, which includes Brillouin lasing, was limited to 2.3 % due to the short cavity length and the relatively small cavity finesse.

Our simulations highlight the importance of the gain detuning parameters $\delta\Omega_j$, even if the pumps are non-recirculating. Mode pulling changes the Stokes lasers frequency, and hence changes their respective detuning from the closest cavity mode, which is a key parameter in setting the comb's dynamics [34]. First, having asymmetric pump detunings $\delta\Omega_{1,2}$ significantly affects the spectral width and symmetry of the comb, as shown in fig. 5f. To maximize the comb bandwidth, the frequency spacing of the pumps $\Delta\omega_p$ must be kept commensurate with the cavity's FSR, similar to pulse pumping schemes [35]. Second, even when $\Delta\omega_p$ is an exact multiple of the FSR, increasing both detunings $\delta\Omega_{1,2}$ toward the red helps to expand the comb (see fig. 5g).

multimode lasing and limitations

Operating the Stokes lasers in the multimode regime leads to a strong degradation in comb coherence, as depicted in fig. 6. The resulting comb is characterized by a rapid decline in power per line and a higher noise floor on the optical spectrum analyzer. The measured beatnotes exhibit broader and multi-peaked characteristics. As the Stokes pumps fluctuate across several cavity modes, each comb line comprises sub-peaks spaced by the cavity's FSR, regardless of the cavity dispersion. This undesirable feature makes such a regime unsuitable for many applications. Consequently, the simulation-experiment agreement also deteriorates, as the chaotic behavior of the Stokes lasers is not taken into account in our model. We found that adding pump power and detuning fluctuations into our model and averaging the resulting combs provides a closer match to the experiments, as shown in fig. 6d.

Mode hopping and multimode lasing are the two main limitations in coherent Brillouin-Kerr comb generation. First, they limit the usable detuning range, thus restricting the accessible comb states within the Brillouin laser. For example, states (i) and (v) shown in figs. 5f,g are unrealistic in practice, since they lie at the extrema $\delta\Omega_{1,2} = \pm D_1/2$, where mode hop occurs. Moreover, at higher pump power, the detuning range for coherent comb generation shrinks.

Beyond a power level $P_{\max}$, both Stokes lasers oper-

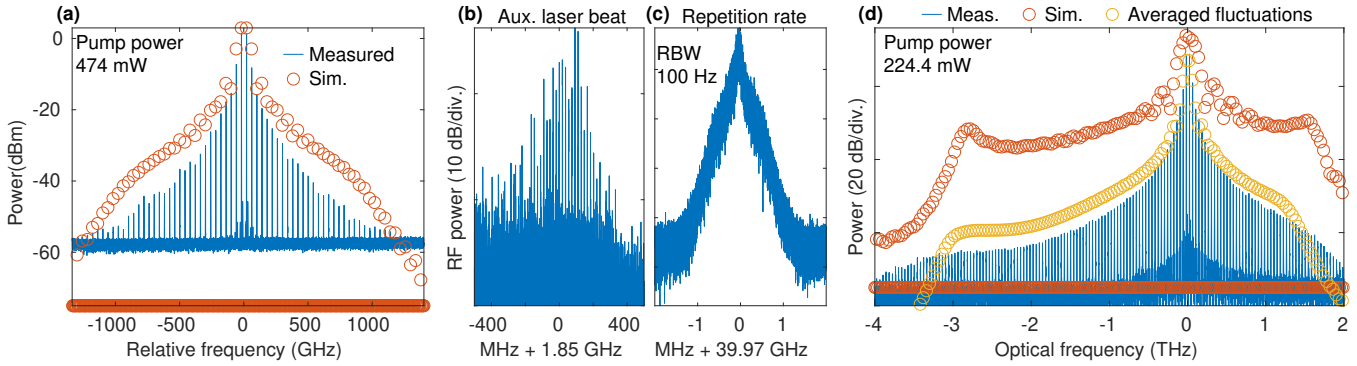

Figure 6: **multimode lasing and comb noise**. **(a)** Optical spectrum of a comb in the multimode Brillouin lasing regime (cavity A). The pump power is 474 mW. The simulations are performed in steady state and do not account for the instabilities. **(b)** RF beatnote of comb line −10 with a reference auxiliary laser (RBW 39 kHz). The multiple peaks result from the multimode operation. **(c)** Comb's repetition rate beatnote, evidencing the low coherence. **(d)** Optical spectrum of a comb in cavity B in the multimode regime, for a pump power of 224.4 mW. The asymmetric comb shape is due to the third-order dispersion. Red dots mark the simulated comb with static parameters ($\delta\Omega_j = 0$). The yellow dots are obtained by averaging 1120 spectra, computed while the power and detuning fluctuate randomly in the range $[0, 225]$ mW and $[-D_1, D_1]$ respectively.

ate only in multimode emission. This maximum power depends on a few factors [23, 36], the most prominent being the cavity's FSR compared to the Brillouin gain bandwidth. The factor $M = \Gamma_B/D_1 \propto L_{\text{tot}}$ relates to the number of modes under the gain curve. The transition of the Stokes laser to multimode, due to optical mode competition over a common acoustic field (homogeneous saturation), can be modeled with dynamical equations [37]. Hence it is difficult to devise an accurate estimate for $P_{\max}$, but a coarse scaling law can be established based on the gain of the adjacent modes

$$\frac{P_{\max}}{P_{th}^{j}} \approx 1 + \left[2\frac{D_1}{\Gamma_B}\right]^2 \tag{9}$$

$$P_{th}^{j} = \frac{A_{\text{eff}}\,\kappa}{g_B\,2c} \approx \frac{A_{\text{eff}}}{g_B}\frac{D_1\,[1-\eta\,(1-\theta)]}{2\pi c} \tag{10}$$

where P_{th}^{j} is the lasing threshold [36] (assuming the gain is on resonance, $\delta\Omega_j = 0$). Note that the above expression would hold for an inhomogeneous saturation, and presently underestimates $P_{\max}$, as mode competition and hysteresis, which tend to extend single-mode operation of an initially lasing mode, are neglected.

Figure 1c maps the relations in eq. (9), to illustrate our discussion. $P_{\max}$ increases with the FSR. In our study, we measured $P_{\max} \sim 220$ mW in the 60 m-long cavity B, and $P_{\max} \sim 470$ mW in the 10 m-long cavity A. Beyond a critical length, there is no single-mode Stokes emission. In contrast, short cavities preserve high-coherence single-mode operation over a wider range of power. Such cavities also enable access to a wider span of detuning, and hence a larger variety of comb states, such as dissipative Kerr soliton states in the anomalous dispersion regime, which appear at relatively large detuning [38]. Our simulations in the anomalous dispersion regime (same parameters used and $\delta\Omega_1 = \delta\Omega_2$, but $D = 16\,\text{ps}\,\text{km}^{-1}\,\text{nm}^{-1}$) indicate that soliton formation occurs for a Stokes laser detuning larger than $\delta\omega_{\text{Stokes1,2}} \gtrsim 0.49\,\kappa/2$. Following the frequency pulling eq. (8), and assuming the maximum Brillouin gain detuning $\delta\Omega_{1,2} = D_1/2$, this condition sets a minimum cavity FSR of $D_1 > \dfrac{\Gamma_B}{1/0.49 - 1/F}$ for soliton formation, where $F = D_1/\kappa$ is the cavity finesse. With the current parameters (assuming that F is constant), this corresponds to an FSR of 26 MHz, i.e. a maximum cavity length of ∼8 m. However, shorter cavities exhibit a higher lasing threshold and a lower accumulated nonlinearity. Indeed, in fiber cavities, the losses are dominated by lumped elements, such that the finesse remains limited and the threshold increases with FSR. Microresonators feature high finesse and nonlinearity, thus circumventing most of these shortcomings and allow soliton-based combs [6, 7], but require the Brillouin pump to be on resonance and precise matching of the cavity's FSR with the Stokes shift, which complicates fabrication, pumping efficiency, and detuning control.

OUTLOOK

In conclusion, the generation of high repetition rate combs in a fiber Brillouin laser cavity has multiple potential advantages in terms of reconfigurability, pump coupling efficiency, and coherence. However, one must be aware of the limitations imposed by the Brillouin laser dynamics in terms of detuning control and coherence degradation, especially in long fiber cavities. We believe that our modeling and observations provide valu-

able insights into the comb states reported in refs. [4, 5], where fibers with lengths ranging from 300 m to 500 m were utilized. Interestingly, we can also extend the conclusions of our analysis to a greater number of pumps, as used in ref. [5]. Preserving coherent operation in a multi-pump scenario likely requires even more stringent constrains on matching the pump spacing with the FSR. Moreover, the Brillouin phonon frequency variation with wavelength would intrinsically induce unequal pump detunings, making it harder to maintain coherent operation. Further analysis of other cavity parameters, such as the dispersion regime, will be the subject of another publication.

The authors acknowledge support from French program "Investments for the Future" operated by the National Research Agency (EIPHI Graduate School, contract ANR-17-EURE-0002), and from Région Bourgogne Franche-Comté and European Regional Development Fund.

[1] Scott A Diddams, Kerry Vahala, and Thomas Udem, "Optical frequency combs: Coherently uniting the electromagnetic spectrum," Science **369**, eaay3676 (2020).

[2] Nathalie Picqué and Theodor W. Hänsch, "Frequency comb spectroscopy," Nature Photonics **13**, 146–157 (2019).

[3] Tobias J Kippenberg, Alexander L Gaeta, Michal Lipson, and Michael L Gorodetsky, "Dissipative Kerr solitons in optical microresonators," Science **361**, eaan8083 (2018).

[4] Qing Li, Zhi-xu Jia, Zhen-rui Li, Yue-de Yang, Jin-long Xiao, Shao-wu Chen, Guan-shi Qin, Yong-zhen Huang, and Wei-ping Qin, "Optical frequency combs generated by four-wave mixing in a dual wavelength Brillouin laser cavity," AIP Advances **7**, 075215 (2017).

[5] Yali Huang, Qing Li, Junyuan Han, Zhixu Jia, Yongsen Yu, Yuede Yang, Jinlong Xiao, Jiliang Wu, Daming Zhang, Yongzhen Huang, Weiping Qin, and Guanshi Qin, "Temporal soliton and optical frequency comb generation in a Brillouin laser cavity," Optica **6**, 1491 (2019).

[6] Yan Bai, Menghua Zhang, Qi Shi, Shulin Ding, Yingchun Qin, Zhenda Xie, Xiaoshun Jiang, and Min Xiao, "Brillouin-Kerr Soliton Frequency Combs in an Optical Microresonator," Physical Review Letters **126**, 063901 (2021).

[7] In Hwan Do, Dohyeong Kim, Dongin Jeong, Daewon Suk, Dohyeon Kwon, Jungwon Kim, Jae Hoon Lee, and Hansuek Lee, "Self-stabilized soliton generation in a microresonator through mode-pulled Brillouin lasing," Optics Letters **46**, 1772 (2021).

[8] M. R. Shirazi, S. W. Harun, K. Thambiratnam, M. Biglary, and H. Ahmad, "New Brillouin fiber laser configuration with high output power," Microwave and Optical Technology Letters **49**, 2656–2658 (2007).

[9] Gwennaël Danion, Ludovic Frein, Denis Bacquet, Grégoire Pillet, Stéphanie Molin, Loïc Morvan, Guillaume Ducournau, Marc Vallet, Pascal Szriftgiser, and Mehdi Alouini, "Mode-hopping suppression in long Brillouin fiber laser with non-resonant pumping," Optics Letters **41**, 2362 (2016).

[10] Sarat Gundavarapu, Grant M Brodnik, Matthew Puckett, Taran Huffman, Debapam Bose, Ryan Behunin, Jianfeng Wu, Tiequn Qiu, Cátia Pinho, Nitesh Chauhan, Jim Nohava, Peter T Rakich, Karl D Nelson, Mary Salit, and Daniel J Blumenthal, "Sub-hertz fundamental linewidth photonic integrated Brillouin laser," Nature Photonics **13**, 60–67 (2019).

[11] Alexis Debut, Stéphane Randoux, and Jaouad Zemmouri, "Linewidth narrowing in Brillouin lasers: Theoretical analysis," Physical Review A **62**, 023803 (2000).

[12] T. Hansson and S. Wabnitz, "Bichromatically pumped microresonator frequency combs," Physical Review A **90**, 013811 (2014).

[13] Kensuke Ikeda, "Multiple-valued stationary state and its instability of the transmitted light by a ring cavity system," Optics Communications **30**, 257–261 (1979).

[14] Tobias Hansson and Stefan Wabnitz, "Dynamics of microresonator frequency comb generation: Models and stability," Nanophotonics **5**, 231–243 (2016).

[15] Jacek Kierzenka and Lawrence F. Shampine, "A BVP solver based on residual control and the Maltab PSE," ACM Transactions on Mathematical Software **27**, 299–316 (2001).

[16] Liang Chen and X Bao, "Analytical and numerical solutions for steady state stimulated Brillouin scattering in a single-mode fiber," Optics Communications **152**, 65–70 (1998).

[17] Mark Dong and Herbert G. Winful, "Unified approach to cascaded stimulated Brillouin scattering and frequency-comb generation," Physical Review A **93**, 043851 (2016).

[18] Thomas F. S. Büttner, Irina V. Kabakova, Darren D. Hudson, Ravi Pant, Christopher G. Poulton, Alexander C. Judge, and Benjamin J. Eggleton, "Phase-locking and Pulse Generation in Multi-Frequency Brillouin Oscillator via Four Wave Mixing," Scientific Reports **4**, 5032 (2014).

[19] Moise Deroh, Bertrand Kibler, Hervé Maillotte, Thibaut Sylvestre, and Jean-Charles Beugnot, "Large Brillouin gain in Germania-doped core optical fibers up to a 98 mol% doping level," Optics Letters **43**, 4005 (2018).

[20] J. I. Thorpe, K. Numata, and J. Livas, "Laser frequency stabilization and control through offset sideband locking to optical cavities," Optics Express **16**, 15980 (2008).

[21] P.-A. Nicati, K. Toyama, S. Huang, and H.J. Shaw, "Frequency pulling in a Brillouin fiber ring laser," IEEE Photonics Technology Letters **6**, 801–803 (1994).

[22] Jiang Li, Hansuek Lee, Tong Chen, and Kerry J Vahala, "Characterization of a high coherence, Brillouin microcavity laser on silicon," Optics Express **20**, 20170 (2012).

[23] V. Lecoeuche, S. Randoux, B. Ségard, and J. Zemmouri, "Dynamics of stimulated Brillouin scattering with feedback," Quantum and Semiclassical Optics: Journal of the European Optical Society Part B **8**, 1109–1145 (1996).

[24] V Lecoeuche, B Ségard, and J Zemmouri, "Modes of destabilization of Brillouin fiber ring lasers," Optics Communications **134**, 547–558 (1997).

[25] Carlos Montes, Derradji Bahloul, Isabelle Bongrand, Jean Botineau, Gérard Cheval, Abdellatif Mamhoud, Eric Picholle, and Antonio Picozzi, "Self-pulsing and dynamic bistability in cw-pumped Brillouin fiber ring lasers," Journal of the Optical Society of America B **16**, 932 (1999).

[26] Hongpu Li and Kazuhiko Ogusu, "Instability of Stimulated Brillouin Scattering in a Fiber Ring Resonator," Optical Review **7**, 303–308 (2000).

[27] B. S. Kawasaki, D. C. Johnson, Y. Fujii, and K. O. Hill, "Bandwidth-limited operation of a mode-locked Brillouin parametric oscillator," Applied Physics Letters **32**, 429–431 (1978).

[28] I. Bar-Joseph, A. Dienes, A. A. Friesem, E. Lichtman, R. G. Waarts, and H. H. Yaffe, "Spontaneous mode locking of single and multi mode pumped SBS fiber lasers," Optics Communications **59**, 296–298 (1986).

[29] S. P. Smith, F. Zarinetchi, and S. Ezekiel, "Narrow-linewidth stimulated Brillouin fiber laser and applications," Optics Letters **16**, 393–395 (1991).

[30] V Lecœuche, D. J Webb, C. N Pannell, and D. A Jackson, "Brillouin based distributed fibre sensor incorporating a mode-locked Brillouin fibre ring laser," Optics Communications **152**, 263–268 (1998).

[31] Luís C. B. Silva, Carlos A. F. Marques, Marcelo E. V. Segatto, and Maria J. Pontes, "Stable self-pulsing regime in a Brillouin ring fiber laser cavity," Laser Physics **31**, 055103 (2021).

[32] Dmitry V. Strekalov and Nan Yu, "Generation of optical combs in a whispering gallery mode resonator from a bichromatic pump," Physical Review A **79**, 041805 (2009).

[33] Bruno Garbin, Yadong Wang, Stuart G Murdoch, Gian-Luca Oppo, Stéphane Coen, and Miro Erkintalo, "Experimental and numerical investigations of switching wave dynamics in a normally dispersive fibre ring resonator," The European Physical Journal D **71**, 240 (2017).

[34] Erwan Lucas, Hairun Guo, John D. Jost, Maxim Karpov, and Tobias J. Kippenberg, "Detuning-dependent properties and dispersion-induced instabilities of temporal dissipative Kerr solitons in optical microresonators," Physical Review A **95**, 043822 (2017).

[35] Ewelina Obrzud, Steve Lecomte, and Tobias Herr, "Temporal solitons in microresonators driven by optical pulses," Nature Photonics **11**, 600–607 (2017).

[36] S. Randoux, V. Lecoeuche, B. Ségard, and J. Zemmouri, "Dynamical analysis of Brillouin fiber lasers: An experimental approach," Physical Review A **51**, R4345–R4348 (1995).

[37] V. Lecoeuche, S. Randoux, B. Ségard, and J. Zemmouri, "Dynamics of a Brillouin fiber ring laser: Off-resonant case," Physical Review A **53**, 2822–2828 (1996).

[38] François Leo, Stéphane Coen, Pascal Kockaert, Simon-Pierre Gorza, Philippe Emplit, and Marc Haelterman, "Temporal cavity solitons in one-dimensional Kerr media as bits in an all-optical buffer," Nature Photonics **4**, 471–476 (2010).